Ultrasonic Measurements of the Elastic Properties of Impacted Laminate Composites

B. TITTMANN and C. MIYASAKA, Penn State University, University Park, PA, USA
H. KASANO Takushoku University, Tokyo, Japan

Abstract. The studies of ultrasonic wave propagation in fiber-reinforced laminates comprise many techniques. This study is to experimentally evaluate the effects of the impact-induced damages of Carbon Fiber Reinforced Plastic (CFRP) laminated composites under no stress and pre-stress conditions. A mechanical scanning acoustic reflection microscope (SAM: pulse-wave mode) was used to detect and evaluate interior damage (e.g., delamination) of the impact-induced specimens.

The studies show that ultrasound provides an attractive means for non-invasive evaluation and thereby a means for understanding the results of high-velocity impact upon laminate composites.

Introduction

The objective of this study is to experimentally evaluate the effects of the impact-induced damages of Carbon Fiber Reinforced Plastic (CFRP) laminated composites under no stress and pre-stress conditions such as (1) no loading, (2) compressive loading, and (3) tensile loading. The symmetrical 4-points bending apparatus was designed and manufactured for making the pre-stressed conditions. Four kinds of test specimens having laminate configurations of $(0_{12}/\theta_{20}/0_{12})$ were employed, wherein their ply angles (denoted as "θ") were 30°, 45°, 60°, and 90°. The test specimens were impacted with an air-gun type of impact apparatus. First, a strain change caused by the impact was measured. Second, a mechanical scanning acoustic reflection microscope (SAM: pulse-wave mode) was used to detect an interior damage (e.g., delamination) of the impact-induced specimens.

The impact-induced damage is the most serious type of damage for carbon fiber reinforced composites [1]. In particular, delamination caused by impact loading is known to produce significant reductions in the residual compression strength (*i.e.*, CAI strength) of carbon fiver reinforced plastic (hereinafter called simply "CFRP") laminated composites, which is a major problem associated with the structural integrity of composite compression components. Therefore, much effort has been devoted to the study of the effects of impact-induced damage on the load-bearing capacities of these components in the past 30 years [2]-[6]. In the course of these studies, attempts have also been made to investigate the damage mechanism [7]-[14]. However, there are a few reports of the impact-induced damage analysis for the CFRP laminates [15]-[17]. In this article we, first, have completed impact tests with the CFRP laminates under pre-stress, second, nondestructively visualized delaminations located at interfaces with scanning acoustic microscopy, third, analyzed strain change caused by the impact.

2. Sample Preparation

The CFRP specimens were fabricated from pre-impregnated sheets (prepregs) having uni-directional long carbon fibers (Nippon Steel Chemical Co., Ltd., Code No A25000) with epoxy matrices. Table 1 shows properties of fibers and matrices of composites used in this study. The specimens were designed to have two interfaces (*i.e.*, interfaces A and B). In this way, two delaminations at interfaces might be introduced by the impact (see Fig. 1). The prepregs were layered up for forming laminated panels in the stacking sequence as shown in Table 2. We fabricated four types of specimens represented by C30, C45, C60, and C90. A subscript number with a denotation is the number of prepregs. Then, the panels were processed using autoclave-molding technique. After the mould was removed, the panels were cut into specimens. The shape of each specimen was rectangular and the dimensions were 180.0mm by 50.0mm with an average thickness of 5.6mm.

Table 1: Properties of Fiber and Matrix

Carbon Fiber		Matrix	
Tensile Strength	3.92GPa	Tensile Strength	2.16GPa
Tensile Elasticity	235GPa	Tensile Elasticity	137GPa
Fiber Diameter	7μm	Bending Strength	1.96GPa
Density	1.78g/cm^3	Bending Elasticity	127GPa
		Compressive Strength	1.41GPa
		Compressive Elasticity	127GPa

Table 2: Stacking Sequence of Specimens

C30	$0^o_{12}/30^o_{20}/0^o_{12}$
C45	$0^o_{12}/45^o_{20}/0^o_{12}$
C60	$0^o_{12}/60^o_{20}/0^o_{12}$
C90	$0^o_{12}/90^o_{20}/0^o_{12}$

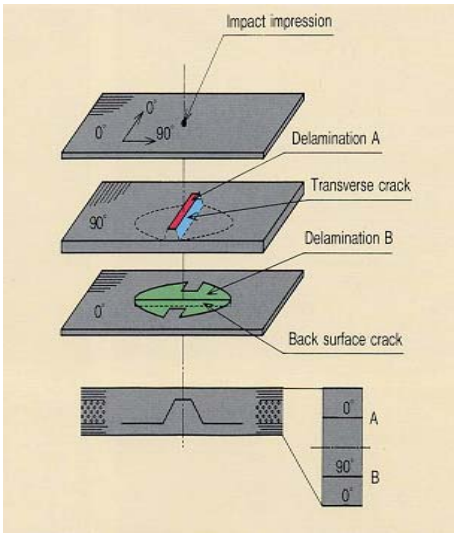

Fig. 1. Schematic diagram of CFRP structure for the specimen denoted as C90. The delaminations at interfaces A and B are named "Delamination A" and "Delamination B."

3. Impact Testing

3.1 Air-Gun Type of Apparatus with Strain Measuring System

Impact tests were performed using an air-gun type of apparatus (see Fig. 2). Air was blown from a supply line into a cylindrical reservoir. A steel ball (diameter: 10.0mm, weight: 4.1g) was used as the impactor. The steel ball was accelerated by compressed air discharged from the reservoir. The impact machine had a velocity-measuring device at the end of the gun barrel. When the steel ball traveled through this device, laser beams were emitted by photodiodes onto the ball to interrupt, and triggered by an electronic counter. The impact velocity was calculated from the distance between the photodiodes and the time intervals between beam interruptions. The impact velocity was controlled by adjusting the air pressure in the reservoir. In the impact test, each specimen was damaged by the steel ball propelled normal to the center of the surface at the desired impact velocity or energy levels. The strain was measured by the strain measuring system through the strain gage attached onto the specimen.

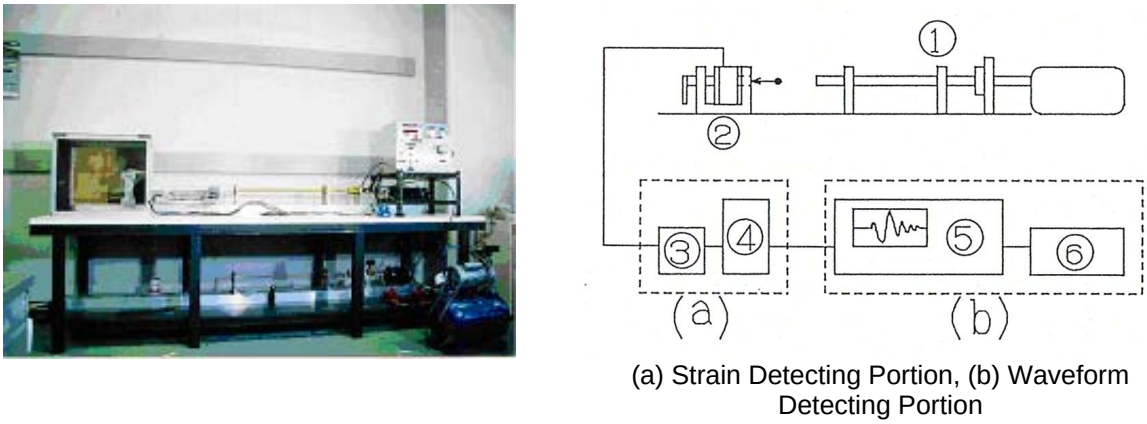

Fig. 2. Schematic diagram of an air-gun type of impact apparatus
1 Air-Gun Type of Apparatus, 2 Unsymmetrical 4-point Bending Apparatus, 3 Bridge Box, 4 Strain Measuring Apparatus, 5 Digital Oscilloscope, 6 Printer

3.2 Unsymmetrical 4-Points Bending Apparatus

The specimen may be pre-stressed by the unsymmetrical 4-points bending apparatus (see Fig.3). When applying the apparatus for bending the CFRP specimen, one surface of the specimen has a pure bending compressive stressed portion, and another surface has a pure bending tensile stressed portion by a predetermined bending moment. The loading force to the specimen from the load cell can be controlled by the strain measuring apparatus.

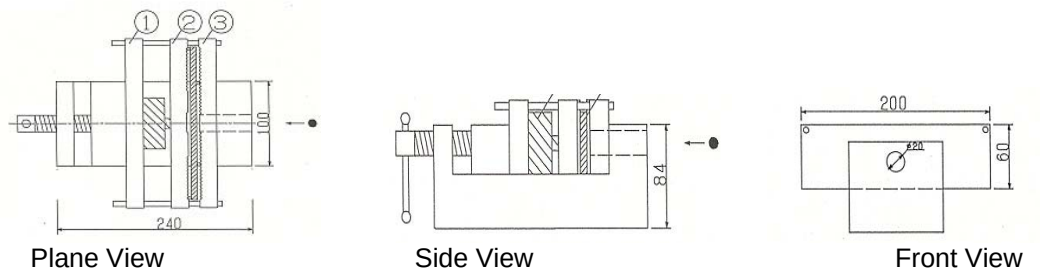

Fig. 3. Schematic diagram of the unsymmetrical 4-Points Bending Apparatus
Plates 1, 2, and 3 are precision plates (S55C). The plates 2 and 3 include 90º-V-notches (depth: 2.0mm) for every 4mm length in longitudinal direction to fix a position of a pin (diameter: 6.0mm). The external span size was 144.0mm, and the internal span size was 48.0mm

3.3 Test Conditions

The specimens were impacted under three different test conditions (see Fig. 4). The steel ball was propelled at the velocity of 40m/s.

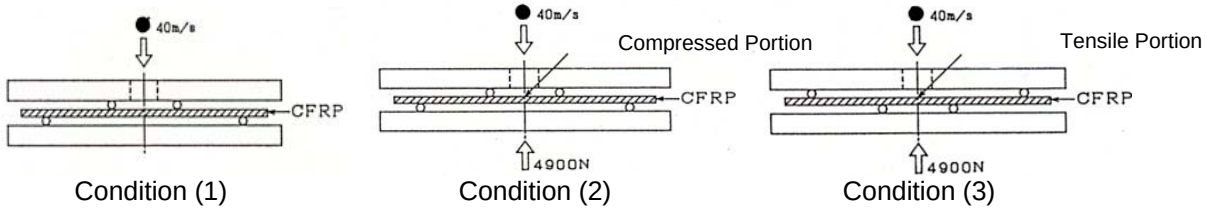

Fig. 4. Condition (1): Impact the steel ball (diameter: 10mm; velocity: 40m/s; air pressure: 4.9×10^4Pa) onto the surface of the CFRP without loading. Condition (2): Impact the steel ball onto the surface including compressed portion with loading (4900N). Condition (3): Impact the steel ball onto the surface including tensile portion with loading (4900N).

4. Acoustic Microscopy

The impact-damaged specimens were nondestructively inspected by the pulse-wave mode of the mechanical scanning acoustic reflection microscope (hereinafter called simply "SAM"). Figure 5 is the schematic diagram of the SAM (Olympus Corporation; model: UH Pulse 100).

4.1. Imaging Principle

An electrical signal is generated by a transmitter/receiver. The electrical signal is transmitted to a piezoelectric transducer (*i.e.*, $LiNb_2O_3$) located on the top of a buffer rod (*i.e.*, Fused Quartz) through the SPDT switch. The electrical signal is converted to an acoustic signal (*i.e.*, ultrasonic plane wave) at the transducer. The ultrasonic plane wave travels through the buffer rod to a spherical recess (hereinafter called simply the "lens") located at the bottom of the buffer rod. The lens converts the ultrasonic plane wave to an ultrasonic spherical wave (*i.e.*, ultrasonic beam). The ultrasonic beam is focused within the specimen, and reflected from the specimen. The reflected ultrasonic beam, which carries acoustic information of the specimen, is again converted to an ultrasonic plane wave by the lens.

Suppose a pulse-wave emitted from an acoustic lens through a coupling media (*e.g.*, water) is focused onto the back surface of the specimen (*i.e.*, CFRP). Suppose the pulse-wave is strong enough to travel through the specimen and reflect back to the acoustic lens. Since the specimen is a layered material, timing of each reflection is different because the traveling distance is different. An oscilloscope may monitor both the amplitude and the delay of the pulse-wave reflected from each plane of the specimen. Note that an output of an electrical pulse signal generated from a transmitter/receiver is approximately 50~300V. The pulse wave can be focused through the specimen of interest for obtaining an optimized acoustic image in quality. For example, when the first interface needs to be clearly visualized to detect a defect such as a delamination, the pulse-wave is focused onto the first interface for maximizing the amplitude of the pulse wave reflected from the first interface. Then, the reflected pulse wave is electrically gated out for visualizing the first interface as a horizontal cross-sectional image by horizontally scanning the acoustic lens.

4.2. Imaging Analysis (Delamination)

Figure 6 is superimposed horizontal cross-sectional acoustic images (C-scan images) showing delaminations at the interfaces A and B of the specimen C60, wherein the images

were formed with frequency at 30MHz. From the images, the delaminations at interfaces B of the hybrid specimens are larger than that of C. The delamination area at interface B was larger than that at interface A. The delaminations at the interfaces A and B were developed along directions (*i.e.*, 60º and 90º) of fibers in front and rear layers, respectively. Using the same method, we visualized the delaminations of the specimens C30, C45, and C90. Areas of delamination introduced by the steel ball impact in different conditions were calculated and compared to determine the relationship between the ply angle and the size of the delamination (see Fig.7).

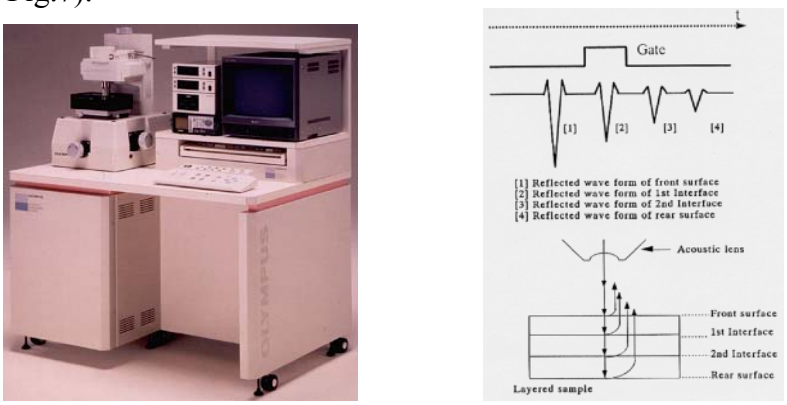

(a) (b)

Fig. 5. (a) A schematic diagram of a mechanical scanning acoustic reflection microscope (SAM; pulse-wave mode). The SAM operates with frequencies ranging from 5MHz to 250MHz. (b) Ultrasonic waves reflected from the specimen. The "gate (*i.e.*, rectangular electrical signal)" was multiplied to the signal reflected from the interface B to visualize a horizontal cross-sectional acoustic image (C-scan Image) at the interface A.

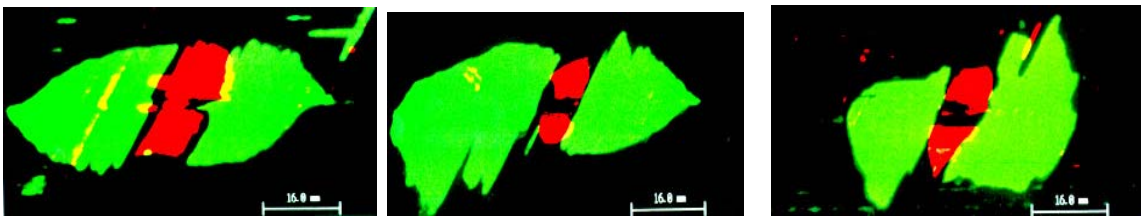

(a) (b) (c)

Fig. 6. Acoustic images show delaminations at interfaces A and B of the specimen C60, wherein the delaminations were introduced by the steel ball impact. The images were formed by the acoustic lens for pulse wave mode with the frequency at 30MHz. (a): Delaminations introduced without loading, (b): Delaminations introduced under compressive loading, (c): Delaminations introduced under tensile loading.

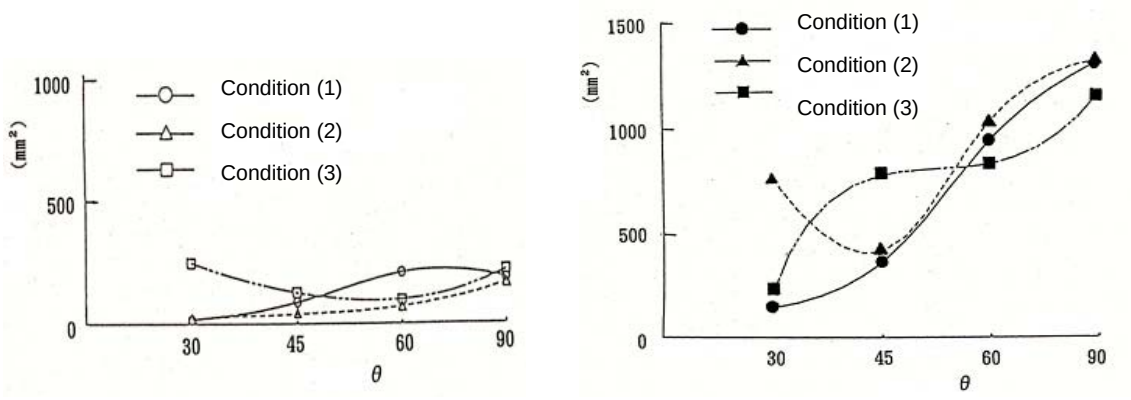

(a) Interface A (b) Interface B

Fig. 7. Delamination area versus ply angle

The delamination area at interface A tends to increase a little in accordance with the increase of the ply angle. On the other hand, the delamination area at interface B tends to rapidly increase.

5. Strain Analysis

Figures 8(a), 8(b), and 8(c) show stain changes of the rear surface of the CFRP specimens categorized in C60 under three different conditions; (1) no loading, (2) compressed loading, and (3) tensile loading. The compressive strain is clearly observed in all the conditions. Moreover, the same trends could be observed for all types of the specimens used in this study.

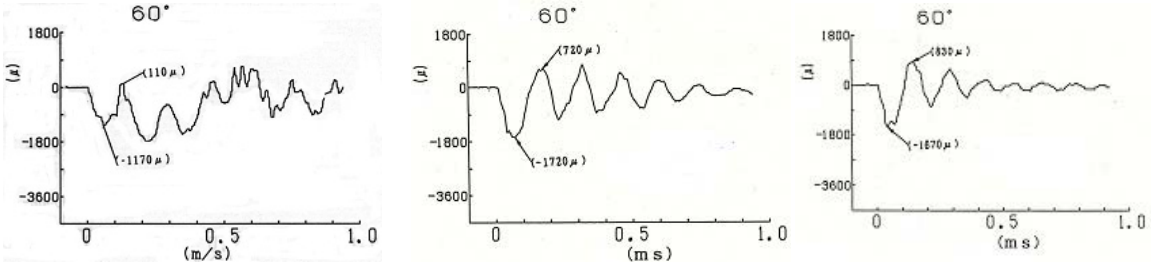

(a) Condition (1) (b) Condition (2) (c) Condition (3)

Fig.8. Strain change of rear surface at impact

Figure 9(a), 9(b) and 9(c) show relations between the strain peaks and the ply angles in three different conditions; (1) no loading, (2) compressed loading, and (3) tensile loading. When the impact is induced to the surface having a compressed portion, both compressive and tensile peak values increase in accordance with the increase of the ply angle.

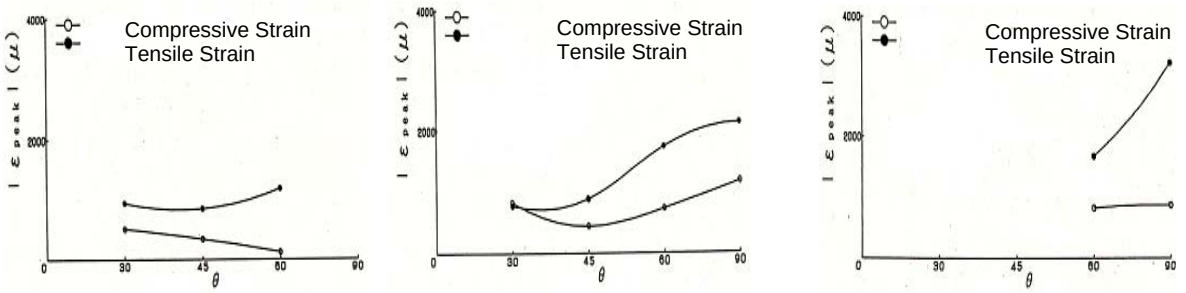

(a) Condition (1) (b) Condition (2) (c) Condition (3)

Fig. 9. Strain peak versus ply angle

6. Conclusion

1. When the impacts were induced onto the surface of CFRP under three different conditions: (1) no loading, (2) compressed loading, and (3) tensile loading, areas of generated delaminations were approximately the same.
2. The delamination at interface A develops along the direction of fibers included in the middle layers. The delamination at interface B develops along the direction of the fibers included in the rear layers.
3. The area of delamination generated by the impact depends on the ply angle. The larger the angle is, the larger is in the area of delamination.
4. The compressive strain is clearly observed in all the cases for all the specimens.

5. When the impact is induced to the surface having a compressed portion, both compressive and tensile peak values increase in accordance with the increase of the ply angle.

References

1. Challenger, K.D., The Damage Tolerance of Carbon Fiber Reinforced Composites-A Workshop Summary, Composite Structures, Vol. 6, pp. 295-318, 1986.
2. Starnes, J.H., Jr., Rhodes, M.D., & Williams, J.G., Effect of Impact Damage and Holes on the Compressive Strength of a Graphite/Epoxy Laminate, ASTM STP696, 1979, pp. 145-171.
3. Sharma, A. V., Low-Velocity Impact Tests on Fibrous Composite Sandwich Structures, ASTM STP734, 1981, pp. 54-70.
4. Labor, J. D., Impact Damage Effects on the Strength of Advanced Composites, ASTM STP696, 1979, pp. 172-184.
5. Williams, J. D., Rhodes, M. D., Effect of Resin on Impact Damage Tolerance of Graphite/Epoxy Laminates, ASTM STP787, 1982, pp. 450-480.
6. Sharma, A. V., Effect of Specimen Size on the Buckling Behavior of Laminated Composites Subjected to Low-Velocity Impact, ASTM STP808, 1983, pp. 140-154.
7. Rhodes, M. D., Williams, J. G., Starnes, J. H., Jr., Low Velocity Impact Damage in Graphite-Fiber Reinforced Epoxy Laminates, Polymer Composites, Vol. 2, No. 1, pp. 36-44, 1981.
8. Takeda, N., Sierakowski, R. L., & Marvern, L. E., Microscopic Observations of Cross-Sections of Impacted Composites Laminates, Composite Technology Review, Vol. 41, No. 1, pp. 40-44, 1982.
9. Malvern, L. E., Sierakowski, R. L., & Ross, C. A., Impact Failure Mechanisms in Fiber Reinforced Composite Plates, Proc. IUTAM, 1977, pp. 24-27.
10. Chai, H., Knauss, W. G., & Babcock, C. D., Observation of Damage Growth in Compressively Loaded Laminates, Experimental Mechanics, Vol. 23, pp. 329-337, 1983.
11. Joshi, S. P., Sun, C. T., Impact-Induced Fracture in a Laminated Composite, Journal of Composite Materials, Vol. 9, pp. 51-56, 1986.
12. Cantwell, W. J., Curtis, P. T., & Morton, J., An Assessment of the Impact Performance of CFRP Reinforced with High Strain Carbon Fibers, Composites Science and Technology, Vol. 9, No. 2, pp. 40-46, 1987.
13. Joshi, S. P., Sun, C. T., Impact-Induced Fracture in a Quasi-Isotropic Laminate, Journal of Composites Technology & Research, Vol. 9, No. 2, pp. 40-46, 1987.
14. Clark, G., Modeling of Impact Damage in Composite Laminates, Composites, Vol. 20, No. 3, pp. 209-214, 1989.
15. Matsumoto, H., Adachi, T., and Ujihashi, S., Static and Impact Induced Damage of CFRP Laminates, Dainamic Fracture Proceedings of Oji Seminar, P.174-182, Chou Technical Drawing Co., Ltd., 1990
16. Kasano H. and Miyasaka C., "Experimental Study on Impact-Induced Damage in CFRP Laminated Composites with Scanned Image Microscopy", Presented at the 2003 ASME Pressure Vessels and Piping Conference, July 21-24, 2003, Cleveland, OH. *Ultrasonic Nondestructive Evaluation for Material Science and Industries* edited by C. Miyasaka, PVP-Vol. 456, pp.113-118. The American Society of Mechanical Engineers, New York, NY, 2003
17. Kasano H. and Miyasaka C., "Transverse Impact of CFRP Laminates under Static Load of Axial Compression with Scanned Image Microscopy", Presented at the 2003 ASME Pressure Vessels and Piping Conference, July 21-24, 2003, Cleveland, OH. *Ultrasonic Nondestructive Evaluation for Material Science and Industries* edited by C. Miyasaka, PVP-Vol. 456, pp.135-141. The American Society of Mechanical Engineers, New York, NY, 2003